Seasonal clockwise gyration and tilt of the Australian continent chasing the center of mass of the Earth‟s system from GPS and GRACE

Shin-Chan Han

School of Engineering, University of Newcastle, Callaghan, New South Wales, 2308, Australia

Correspondent: Shin-Chan Han (shin-chan.han@newcastle.edu.au)

Journal of Geophysical Research

Revised, 28SEP16

Abstract

As atmosphere, ocean, ice, and terrestrial water are redistributed, the center of mass (CM) of the Earth‟s system moves and the accompanying loading yields global surface deformation. In Australia, when GPS surface displacements were corrected for local mass change (hydrology, atmosphere, and ocean) with GRACE data, the residual GPS data reveal a peculiar seasonal mode of continental deformation. During the southern Summer, the entire continent coherently shifts northwest by ~1 mm and the southeastern part is uplifted, while the northwestern part is subsided by 2-3 mm and the opposite patterns of deformation are observed during the southern Winter. Such characteristic deformation could be understood to be a result of the Earth‟s elastic response to globally-averaged surface mass load, generally heavier in Europe during southern Summer and in the south Pacific Ocean during southern Winter. It was found that such deformation is even larger than local hydrology-induced loading effects in horizontal motion over Australia. A simple method of determining locations of the CM was developed by combining GPS and GRACE data; the latter being insensitive to the CM motion but sufficiently accurate to remove the local hydrologic and atmospheric effects in GPS data. The CM signals are pronounced over systematic errors in GPS and GRACE data. The CM coordinates estimated by inversion of the Australian GPS dataset and GRACE agree with the geocenter motions determined by satellite tracking analysis. This study suggests an independent way of monitoring the CM motion entirely based on two distinct geodetic measurements of GPS and GRACE.

1. Introduction

Mass redistribution within the Earth‟s system (solid body + fluid envelope including atmosphere) perturbs the Earth‟s gravity field through direct effect of mass movement and indirect effect of accompanying load deformation [*e.g.*, *Farrell,* 1972; *Chao et al.*, 1987]. The surface deformations are measured by precision positioning system such as the Global Positioning System (GPS) within a few mm accuracy [*e.g.*, *Blewitt et al*., 2016] and the global gravity changes are continuously measured by Gravity Recovery And Climate Experiment (GRACE) within a couple of 10^{-8} m/s^2 at a spatial scale of ~400 km [*e.g.*, *Han et al*., 2013; *Watkins et al*, 2015]. The GRACE gravity fields are observed with respect to a coordinate system centered at an instantaneous center of mass (CM) of the whole Earth including atmosphere and fluid components. This is implicitly realized by estimating the gravity fields from tracking GRACE satellites orbiting around CM of the Earth. On the contrary, the GPS 3D positions are referenced to a coordinate system such as International Terrestrial Reference Frame (ITRF) with the origin that is not necessarily coincident with CM.

The geocenter motion, a motion of CM with respect to a reference frame realized by establishing the global satellite tracking network, has been best-determined by Satellite Laser Ranging (SLR) techniques [*Pavlis*, 2003]. The origin of such reference frame is (ideally) the center-of-figure (CF) of the Earth, but is practically a center of the network [*Wu et al*., 2012]. The geocenter motion is simultaneously estimated with the SLR orbit and gravity field solutions [*Cheng et al.*, 2010]. *Blewitt et al*. [2001] detected the seasonal cycle of deformation induced by CM migrating on the Earth‟s surface from global GPS data. However, determination of the inter-annual CM motion and its load deformation was difficult since the inter-annual GPS signals are largely related to tectonic motion (not surface loading).

Wu et al. [2002] found that the GPS analysis of CM could be contaminated by sparse distribution of the GPS stations and aliasing of unknown (uncorrected) "high-degree" deformation. *Davis et al.* [2004] found a strong correlation in radial (vertical) displacement between GPS measurements and GRACE-inferred deformation over the Amazon basin with inclusion of the CM-induced radial load displacement in GRACE data.

Kusche and Schrama [2005] and *Wu et al*. [2006] determined global surface mass distribution by combining simultaneously GPS, GRACE, and ocean models. More recent analyses reported substantial correlation between GPS and GRACE at different locations due to different kinds of surface mass loads [*e.g*., *Nahmani et al*., 2012; *Fu et al*., 2013; and references therein]. Most of the studies exploit the CM estimates from various techniques including SLR determination [*Cheng et al*., 2013], GRACE and ocean model estimates [*Swenson et al*., 2008], geophysical model estimates [*Chen et al*., 1999] and/or joint inversion of multiple data sets [*Wu et al*., 2012]. However, there still exists important discrepancies among different estimates from various techniques and geophysical models [*Ries*, 2013].

In this study, I report the regionally-coherent mode of seasonal deformation prevailing over Australia quantified from GPS and GRACE data; the Australian continent undergoes periodic deformation of up to a couple of mm in horizontal component and ~3 mm in vertical component seasonally. It is found that the horizontal motion is even larger than local hydrologic and atmospheric load deformation. Such motions are analyzed considering the CM migration on the Earth‟s surface. This research demonstrates that simple differences between GPS and GRACE can provide meaningful information on load deformation caused by the CM motion. Furthermore, I develop a method to estimate the coordinates of CM motion using a regional set of GPS data combined with GRACE-inferred displacement. The results are compared with the geocenter motions determined from SLR.

2. Center of mass of the Earth's system

The coordinates of CM in a Cartesian coordinates system are defined by a volume integral of product of an infinitesimal mass element *dm* and its location in each coordinate axis (*i.e.*, linear moment) over the Earth, for example, $X_{CM} \equiv \frac{1}{M}\int X dm$ for the *X*-axis. It can be shown that the CM coordinates are directly related to the „degree-1" gravitational potential field as follows [*e.g.*, *Jekeli*, 2015]:

$$X_{CM} \equiv \frac{1}{M}\int X dm = \sqrt{3}a\bar{C}_{1,1}, \quad (1a)$$

$$Y_{CM} \equiv \frac{1}{M}\int Y dm = \sqrt{3}a\bar{S}_{1,1}, \quad (1b)$$

$$Z_{CM} \equiv \frac{1}{M}\int Z dm = \sqrt{3}a\bar{C}_{1,0}, \quad (1c)$$

where $\bar{C}_{1,0}$, $\bar{C}_{1,1}$, and $\bar{S}_{1,1}$ are the degree-1 gravitational potential coefficients. The coefficients are dimensionless and normalized following the convention in *Heiskanen and Moritz* [1966]. The constant, *a* is a radius of the mean Earth"s sphere used to expand the gravitational potential field in terms of a series of spherical harmonic functions.

The degree-1 component of the Earth"s gravitational potential field at time, *t* is written as

$$V_1(\theta,\lambda,t) = \frac{GM}{a}\left\{\bar{C}_{1,0}(t)\bar{P}_{1,0}(\cos\theta) + \bar{C}_{1,1}(t)\bar{P}_{1,1}(\cos\theta)\cos\lambda + \bar{S}_{1,1}(t)\bar{P}_{1,1}(\cos\theta)\sin\lambda\right\}, \quad (2)$$

where G is the gravitational constant, M is total mass of the Earth"s system. $\bar{P}_{1,m}(\cos\theta)$ is the fully-normalized associated Legendre function of degree 1 and order *m* at co-latitude θ. The degree-1 spherical harmonic functions are formed by multiplying sine and cosine

functions of longitude, λ to the associated Legendre function [*Heiskanen and Moritz*, 1966]. The degree-1 potential coefficients ($\bar{C}_{1,0}$, $\bar{C}_{1,1}$, and $\bar{S}_{1,1}$) can be time-dependent as mass redistributes within the Earth‟s system. Most of the time-variable mass change occurs on the Earth‟s surface associated with water, ice, and atmospheric mass redistribution besides solid Earth mass change due to earthquakes, viscous postglacial rebound, and mantle flow.

Assuming mass change occurs entirely as a result of surface mass redistribution and the accompanying loading, the degree-1 component of the surface mass change, which is responsible for gravitational potential change in equation (2) as well as CM change in equation (1), can be expressed in terms of equivalent water height as follows:

$$h_1(\theta,\lambda,t) = a\{\bar{C}^h_{1,0}(t)\bar{P}_{1,0}(\cos\theta) + \bar{C}^h_{1,1}(t)\bar{P}_{1,1}(\cos\theta)\cos\lambda + \bar{S}^h_{1,1}(t)\bar{P}_{1,1}(\cos\theta)\sin\lambda\}, \quad (3)$$

where the dimensionless degree-1 coefficients of equivalent water height, $\bar{C}^h_{1,0}$, $\bar{C}^h_{1,1}$, and $\bar{S}^h_{1,1}$ produce the degree-1 gravitational potential change through $\bar{C}_{1,m} = \frac{\rho_w}{\rho_e}(1+k'_1)\bar{C}^h_{1,m}$ [*e.g.*, *Kusche and Schrama*, 2005] with a mean density of the Earth (ρ_e = 5517 kg/m^3) and a density of water (ρ_w = 1000 kg/m^3). The degree-1 load Love number for gravitational potential k'_1 is given in the coordinate system that identifies the CM change; *e.g.*, k'_1 = 0.021 in the CF system [*Blewitt*, 2003].

Expressing the gravitational potential and equivalent water height changes in terms of the coordinates of CM and explicitly representing the associated Legendre functions, equations (2) and (3) are simplified as

$$V_1(\theta,\lambda,t) = \frac{GM}{a^2}[X_{CM}(t)\sin\theta\cos\lambda + Y_{CM}(t)\sin\theta\sin\lambda + Z_{CM}(t)\cos\theta]. \quad (4)$$

$$h_1(\theta,\lambda,t) = \frac{\rho_e}{\rho_w(1+k'_1)}[X_{CM}(t)\sin\theta\cos\lambda + Y_{CM}(t)\sin\theta\sin\lambda + Z_{CM}(t)\cos\theta]. \quad (5)$$

The only difference between the degree-1 variations of gravitational potential and equivalent water height is a scale factor in front of the brackets in equations (4) and (5). That is, their spatial patterns are identical. It is not necessarily true for higher-degree ($l \geq 2$) components.

The surface mass (terrestrial water storage, atmospheric and oceanic mass) applies loads on the lithosphere and yields surface and interior deformation. *Farrell* [1972] developed a theory on the linear response of elastic deformation to surface mass load in a spectral domain and derived also the response (Green's) functions in a spatial domain. The degree-1 load excites only the degree-1 (elastic) displacement and gravitational potential. The degree-1 surface displacements of u_1 (up), e_1 (east), and n_1 (north) can be expressed as (*e.g.*, *Kusche and Schrama* [2005]):

$$u_1(\theta,\lambda,t) = \frac{h_1'}{(1+k_1')}\{X_{CM}(t)\sin\theta\cos\lambda + Y_{CM}(t)\sin\theta\sin\lambda + Z_{CM}(t)\cos\theta\}, \quad (6)$$

$$e_1(\theta,\lambda,t) = \frac{l_1'}{(1+k_1')}\{-X_{CM}(t)\sin\lambda + Y_{CM}(t)\cos\lambda\}, \quad (7)$$

$$n_1(\theta,\lambda,t) = \frac{l_1'}{(1+k_1')}\{-X_{CM}(t)\cos\theta\cos\lambda - Y_{CM}(t)\cos\theta\sin\lambda + Z_{CM}(t)\sin\theta\}, \quad (8)$$

where h_1' and l_1' are the load Love numbers for vertical and horizontal load displacements; *e.g.*, $h_1' = -0.269$ and $l_1' = 0.134$ in the CF system [*Blewitt*, 2003]. The degree-1 surface deformation of equations (6-8) are due to the degree-1 surface mass, h_1 loading, or alternatively, due to the CM departing from the center of the coordinate system on which the deformation is defined.

It is useful to emphasize that spatial patterns of the degree-1 load, h_1 and its responses in gravitational potential field, V_1 and in vertical displacement, u_1 are identical. However, the responses in horizontal displacements, e_1 and n_1 are distinct each other and from u_1, and

thus three coordinates of degree-1 displacements can provide full constraints on the CM coordinates through equations (6-8). In principle, 3D surface deformation from a single station can provide the complete information on CM motion, if higher-degree ($l \geq 2$) components of the deformation are known and properly removed (such as from GRACE).

3. SLR observations of the center of mass

I examined the CM coordinate estimates (or geocenter motions) determined from the analysis of multiple SLR data. The estimates consist of monthly time-series of „instantaneous" CM coordinates with respect to the SLR stations" coordinate system that is consistent with ITRF2005 [*Cheng et al.*, 2013]. Here, the CM coordinate changes are attributed to mass change on the Earth"s surface and accompanying load deformation. Using equation (5), the monthly mean patterns of the degree-1 surface water load were computed from the SLR"s CM estimates during 2003 to 2015 (Figure 1). Each panel shows a mean spatial pattern of water load, h_1 and of horizontal load displacement vector, (e_1, n_1) every month. The vertical displacement, u_1 should be identical to h_1 except for a scale difference of –0.05 ($\approx h_1'/(\rho_e/\rho_w)$). That is, the degree-1 load corresponding to 40 mm of equivalent water mass yields the degree-1 subsidence of 2 mm.

In January-February (Figure 1), for example, there exists a net surplus of surface mass distribution around Europe and north Africa while a mass deficit is found in the south Pacific Ocean equivalent to 20–30 mm of water. It results in subsidence of 1–1.5 mm over Europe and north Africa and an uplift in the south Pacific Ocean due to the Earth"s elastic response to the surface mass load. There are outward lateral motions of <1 mm away from the south Pacific Ocean and inward motions towards Europe.

The Australian continent happens to be located where horizontal gradients of the degree-1 load, h_1 is largest between the positive and negative peaks and thus undergoes the largest degree-1 horizontal displacements in the world. This calculation in Figure 1 based on the SLR‟s CM estimates predicts that the Australian continent seasonally oscillates by moving towards Europe during (southern) Summer, towards north America during Autumn, towards the south Pacific Ocean during Winter, and towards central Asia during Spring, as a result of seasonal migration of global mean (*i.e.*, degree-1) surface mass.

4. GPS and GRACE observations of the degree-1 load displacement

I analyzed GPS displacement data in Australia to verify the seasonally-oscillating motions predicted from the SLR‟s CM estimates. The 3D daily position data (north, east, and up) of the Australian GPS network, processed by Nevada Geodetic Laboratory, University of Nevada Reno (UNR), were used in this study. The GPS positions were corrected for tidal deformations (body, ocean and pole) and thus imply instantaneous deformation caused by atmosphere, non-tidal ocean, and terrestrial water loads as well as tectonics including earthquakes [*Tregoning et al*., 2013]. The total of 14 Australian stations with longer than 9 years of continuous position solutions to year 2015 were considered. The GPS time-series data include biases in all three components introduced by sporadic equipment changes and earthquakes. The UNR solutions provide the information of the timings of such events for all processed stations. I determined and removed those biases empirically by fitting a function of seasonal sinusoids, linear trend, and offset parameters at the reported offset epochs. In addition, monthly GRACE gravity field data of Release-05 (RL05) Level-2 (L2) products processed by Center for Space Research (CSR), University of Texas, were used [*Bettadpur et al*., 2014]. The atmosphere and ocean models that were removed from the CSR L2 products

were restored in the GRACE data to make GRACE gravity change consistent with GPS deformation [*Dobslaw et al*., 2013]. The L2 spherical harmonic coefficients were used up to degree and order 40 (The effects of different truncations are discussed in Section 6).

Because GRACE gravity changes are referenced to a coordinate system centered at the instantaneous CM of the Earth‟s system, the degree-1 components of GRACE gravity changes in such coordinate system are, by definition, trivial (zeroes). I used the GRACE gravity data to compute 3D load deformation using the elastic load Love numbers after *Farrell* [1972] and *Davis et al*. [2004] in the GRACE context. The difference between GPS-measured and GRACE-inferred displacements should indicate the origin translation to the instantaneous CM from the origin of the GPS coordinate system. The vector $\mathbf{u}_1$ is defined as:

$$\mathbf{u}_1(t) = \mathbf{u}_{GPS}(t) - \mathbf{u}_{GRACE}(t), \tag{9}$$

where $\mathbf{u}_{GPS}$ is the GPS displacement and $\mathbf{u}_{GRACE}$ is the computed displacement using the GRACE L2 coefficients (degree $l \geq 2$).

The vector, $\mathbf{u}_1$ is the degree-1 displacement presumably related to the CM coordinates through equations (6-8). This is true only if gravity changes and surface displacements are strictly due to an elastic deformation by surface mass load. For example, gravity change and displacement by tectonics and earthquakes violate this assumption. The plate motions are generally the most prominent signals measured in the GPS horizontal displacements. GPS observations have shown that the Australian continent steadily moves northeast by ~7 cm/yr quantified in a time scale of a decade or two [*Tregoning*, 2003]. The large earthquakes around the world produce measurable coseismic and postseismic deformation in Australia by interrupting GPS time-series episodically and gradually [*Tregoning et al*., 2013]. Surface mass redistribution (water, snow, ice, and atmosphere) is characterized dominantly at the

seasonal and inter-annual time scales. In practice, removing linear trends in GPS and GRACE data can effectively filter out non-desired tectonic/earthquake signals as well as secular changes in surface mass redistribution [*Blewitt et al*., 2001].

Figure 2 presents the daily observations of east, north, and up components of the degree-1 displacement, $\mathbf{u}_1$ from GPS–GRACE, after de-trending the time-series from all 14 GPS stations considered in this study (GPS site locations are shown in Figure 3). The monthly GRACE data were interpolated into daily intervals of the GPS data. The de-trended degree-1 displacements evaluated at those GPS stations using the SLR"s CM solutions are compared. The parameters of annual and semi-annual sinusoids were used to estimate the seasonal change from each time-series. The seasonal displacements of ~1 mm (±0.03 mm) in horizontal components and of ~2 mm (±0.07 mm) in vertical component are evident in the GPS–GRACE time-series and are consistent with the SLR predicted motions, except larger amplitudes estimated from GPS–GRACE (70, 20, and 40% larger in east, north, and vertical component, respectively). The doubling of the amplitude in vertical CM displacement compared with the horizontal one is consistent with the vertical load Love number, h_1' being double the horizontal number, l_1'. *Wahr et al*. [2013] also found the asymptotic ratio of ~2 between the vertical and horizontal load deformation when the displacement is computed far away from the source mass load.

I also determined the monthly spatial patterns of the degree-1 displacements, $\mathbf{u}_1$ from GPS–GRACE as shown in Figure 3 with arrows indicating horizontal motions and colored dots for vertical motions (positive for uplift). More than 9 years of GPS and GRACE data were stacked and averaged into a monthly interval to estimate monthly snapshots of the 3D displacements. The continent-wide northwest shift in Summer (Dec.-Feb.) and southeast shift in Winter (Jun.-Aug.) are observed. It is also observed that the continent is subject to seasonal vertical motion with the southeastern Australia elevated and the north of Western

Australia lowered by a few mm during Summer and the opposite during Winter, creating the vertical slope („tilt") across the continent by <5 mm over ~3,500 km. These horizontal and vertical motions are indicative of the spontaneous (elastic) responses to surface mass loads imposed around Europe in Summer and in the south Pacific Ocean in Winter following the seasonal migration of the degree-1 load (*i.e.*, CM).

The 3D CM deformation found from GPS–GRACE data (Figure 3) are in general consistent with the SLR results (Figure 1). Two independent data sets suggest that the entire Australian continent tilts northwest in Summer and southeast in Winter, and gyrates as a whole in a clockwise direction, making an elliptical motion seasonally by ~1 mm in the northwest-southeast axis and by a smaller amount in the perpendicular axis, chasing the center of the Earth system"s mass.

Meanwhile, the displacements by the local ($l \geq 2$) hydrology, ocean, and atmosphere loading were computed using the GRACE data and compared with the degree-1 deformation (GPS–GRACE) in Figure 4. Their monthly patterns are shown in Figure 5. It was found that the CM deformation is larger than the local load deformation in the horizontal component, while it is 2-3 times smaller in the vertical displacement. The CM displacement (not hydrology loading) is the most dominant signal characterizing the seasonal horizontal motion in Australia. While the CM displacements were spatially-coherent among different stations, the GRACE local loading data present diverse timings and amplitudes of seasonal variations reflecting spatially-variable atmospheric, oceanic and hydrological load cycles.

5. Center of mass estimated from GPS and GRACE

The CM motions were estimated using the degree-1 displacement data of GPS–GRACE. Equations (6-8) show three independent linear relationships between the CM coordinates and the degree-1 load displacements. They can be re-written as $\mathbf{u}_1 = \quad (\theta,\lambda)\mathbf{X}_{CM}$ where a 3×3 matrix, $\mathbf{R}(\theta,\lambda)$ is determined by the latitudes and longitudes of GPS stations and the degree-1 load Love numbers, (h_1', l_1', and k_1') such as,

$$(\theta,\lambda) = \frac{1}{(1+k_1')}\begin{bmatrix} h_1' & 0 & 0 \\ 0 & l_1' & 0 \\ 0 & 0 & l_1' \end{bmatrix}\begin{bmatrix} \sin\theta\cos\lambda & \sin\theta\sin\lambda & \cos\theta \\ -\sin\lambda & \cos\lambda & 0 \\ -\cos\theta\cos\lambda & -\cos\theta\sin\lambda & \sin\theta \end{bmatrix}. \tag{10}$$

This matrix can be interpreted as a rotation matrix from the geocentric to topocentric coordinate system (also in equation (13) of *Blewitt and Clarke* [2003]), and is successively scaled by the Love numbers. Inversely, the CM coordinates can be computed by converting the degree-1 displacement vectors epoch-by-epoch and station-by-station through inversion of the station-dependent factor, (θ,λ) as follows:

$$\mathbf{X}_{CM}(t) = \quad ^{-\mathbf{1}}(\theta,\lambda)\mathbf{u}_1(t). \tag{11}$$

The procedure taken in this paper is: At each GPS station, the 3D coordinates of GPS displacements are differenced with the GRACE-inferred load displacements to estimate the degree-1 load displacements following equation (9). Monthly GRACE data are interpolated to daily interval to match the GPS sampling. Both GPS and GRACE time-series are de-

trended to eliminate tectonic signals particularly in the horizontal components. Then, equation (11) is used to convert the degree-1 load displacements from each station to obtain the CM coordinates. The time-series of $\mathbf{X}_{CM}$ from multiple GPS stations are combined to estimate the coordinates of the CM motions.

Figure 6 shows the daily time-series of three components of the CM motion, $\mathbf{X}_{CM}$ converted through equation (11) from GPS minus GRACE data, $\mathbf{u}_1$. Unlike the degree-1 displacements at each GPS station, the CM motion coordinates are no longer station-dependent, allowing simple average of all data from different stations to reduce (mostly) GPS data noise in the CM estimates. The daily estimates present a few centimeters of variations rather uniformly in all three coordinates of CM, in contrast to those of the surface CM deformation (Figure 2). The monthly averages of the daily estimates were computed and found to be generally within ±10 mm.

I compared total 12 years of the monthly CM motion estimates from GPS–GRACE with the SLR‟s geocenter solutions after removing the linear trend in the SLR solutions in Figure 7a. The timings of peak and trough occurrences agree well each other in all three components. The seasonality of the Y_{CM} estimates is better characterized from the GPS/GRACE solutions than the SLR‟s Y_{CM} solutions (relevant to the geopotential component of $\bar{S}_{1,1}$ in the SLR orbit and gravity analysis) for the period of 2004–2009. However, the GPS/GRACE solutions become worse in 2010 and beyond. The average monthly changes were also compared by stacking all 12 years of the monthly time-series (Figure 7b). Two independent solutions are consistent; the peak is observed in January, December, and March, respectively, for X_{CM}, Y_{CM}, and Z_{CM}; the trough is found in July, May, and August, respectively, for X_{CM}, Y_{CM}, and Z_{CM}; both data indicate larger variability in X_{CM} and Z_{CM} components than in Y_{CM}. In general, the GPS/GRACE CM solutions present a larger variability than the SLR solutions.

In GPS analysis, non-geophysical signals are often observed at the frequencies of one cycle per the GPS draconitic year (~351.4 days) and of its integer multiples, originating from GPS orbital errors and time-modulation of site dependent multipath [*Ray et al.*, 2008; *Tregoning and Watson*, 2009]. The magnitude can reach up to a few mm [*King and Watson*, 2010]. I examined the frequency contents of two CM coordinate time-series in a spectral domain. Figure 8 shows the amplitude (square root of power) spectral density of each time-series. Both GPS/GRACE and SLR CM solutions present the primary peaks centered at the period of a solar year (~365.25 days) distinguished from the GPS draconitic year. The CM estimates from GPS/GRACE are less contaminated by GPS systematic errors around the annual band. However, GPS/GRACE CM solutions exhibit the secondary peaks at half draconitic year (~175.6 days) as well as at half solar year (for Y_{CM}, only at half draconitic year). The SLR solutions present the peaks at half solar year for X_{CM} and Z_{CM} and none at half draconitic year. Around the semi-annual band, the GPS/GRACE CM solutions are significantly corrupted by GPS specific errors.

The CM estimates can be improved by including additional GPS–GRACE data from other places of the world. The GPS systematic errors may cancel while the CM motions will become more pronounced by stacking global data through equation (11). Different places exhibit different sensitivities to the CM coordinates. The sensitivity is determined by the matrix $^{-\mathbf{1}}(\theta,\lambda)$ of equation (11), which is composed of nine elements like $\partial X_{CM}/\partial u_1$, $\partial Y_{CM}/\partial u_1$, $\partial Z_{CM}/\partial u_1$, $\partial X_{CM}/\partial e_1$, $\partial Y_{CM}/\partial e_1$, $\partial Z_{CM}/\partial e_1$, $\partial X_{CM}/\partial n_1$, $\partial Y_{CM}/\partial n_1$, and $\partial Z_{CM}/\partial n_1$ (*i.e.*, partial derivatives of three CM coordinates with respect to three degree-1 displacements). The analytic expression of each element can be easily found from equation (10). The results are presented in Figure 9. The CM sensitivity is roughly twice larger with respect to the horizontal $\mathbf{u}_1$ displacement.

The X_{CM} is most well constrained by the east component of $\mathbf{u}_1$ from stations around longitudes close to 90°E or 90°W (*e.g.*, America and Asia), by the north component from stations in higher latitudes and longitudes close to 0°E or 180°E (*e.g*, Alaska, the Russian Far East, Iceland, and northern Europe). The vertical component of $\mathbf{u}_1$ from stations in lower latitudes and longitudes close to 0°E or 180°E will also contribute to determine X_{CM}. For Y_{CM}, the east component from stations in Pacific, New Zealand, Africa, UK (longitudes close to 0°E or 180°E), the north component from Canada, Siberia (higher latitudes and longitudes close to 0°E or 180°E), and the vertical component from India and Central America (lower latitudes and longitudes close to 90°E or 90°W) are most sensitive. For Z_{CM}, the north component from the equatorial stations are most sensitive and the vertical component from the polar regions are sensitive as well, however, the east component are not sensitive at all. For an example of the $\mathbf{u}_1$ displacement data from the east coast Australian stations, the vertical, east, and north component is most sensitive to X_{CM}, Y_{CM}, and Z_{CM}, respectively.

6. Errors in GRACE and GPS data processing

Systematic errors associated with GRACE and GPS data processing were examined for their impact on the CM estimation. Although GRACE data are provided degree and order up to 90 (*e.g.*, CSR L2 data) [*Bettadpur et al.*, 2014], the coefficients are valid globally up to ~40 and around the polar regions up to 60 or higher. The spherical harmonic truncation will have an effect on computation of local displacement $\mathbf{u}_{GRACE}$ used to compute $\mathbf{u}_1$. Figure 10a shows the square root of power spectrum per degree (*i.e.*, degree amplitude spectrum) and that of cumulative power per degree for vertical load displacement computed from global models of hydrology [*Rodell et al.*, 2004] and atmosphere and ocean mass variation [*Dobslaw et al.*, 2013]. The global average of vertical load displacement is computed to be several mm.

Figure 10b shows the daily time-series of the synthetic displacements at Alice Spring computed from different degree bands. The contribution from degrees higher than 40 is anticipated to be less than 0.1 mm.

The other major systematic error in GRACE data is a large uncertainty in the second degree zonal harmonic coefficient (J2) estimate. This component of the geopotential field is highly correlated with the GRACE orbital state parameters and poorly constrained by GRACE inter-satellite ranging data [*Han et al*., 2008]. I used the GRGS RL03 solutions of geopotential fields determined using LAGEOS and GRACE tracking data [*Lemoine et al*., 2014]. The J2 component was improved by including LAGEOS laser ranging data. This is the set of the solutions most distinct from other project solutions including CSR, JPL, and GFZ in terms of GRACE data processing strategy. The GRGS solutions were constrained within the least-square inversion and available degree and order up to 80. The difference between GRGS solution (out to degree 80) and CSR solution (truncated to 40) may be a good representation of the upper bound of GRACE processing error including J2 uncertainty as well as spherical harmonic series truncation. Figure 11 shows the difference between two GRACE solutions projected to the CM coordinates. The effect of the J2 difference and truncation in GRACE data are insignificant compared to the CM motion signals (Figure 7).

Tregoning and Watson [2009] and *Steigenberger et al*. [2009] reported that different tropospheric delay modeling may yield systematic difference in GPS position solutions as large as ~1 mm at annual and semiannual periods and found that position solutions can be improved by using Vienna Mapping Function 1 (VMF1) against Global Mapping Function (GMF) [*Boehm et al*., 2006]. To quantify the effect of GPS tropospheric modeling on the CM estimates, I analyzed the difference between two sets of GPS daily solutions from UNR and JPL; the former uses GMF while the latter uses VMF1. Figure 11 also presents the difference between two GPS solutions shown as the difference in the CM coordinate

estimates. The processing differences of GPS and GRACE data are as large as root-mean-square (RMS) of 1.5–2.5 mm in the CM coordinates while the CM motion signals are significantly larger with RMS of 7–8 mm.

7. Discussion

I found that the most dominant signal in horizontal deformation of the Australian continent, beside the (steady) plate tectonic motion, is the elastic load displacement induced by global mean surface mass redistribution (or CM migration). The regular trajectory of seasonal mass migration (a composite of terrestrial water, atmosphere, and ocean loads being heavier over Europe in February and over the south Pacific Ocean in August) excites a peculiar seasonal mode of surface displacements; (1) the Australian continent undergoes seasonal clockwise gyration with an elliptical shape elongated in a northwest-southeast direction with the major axis radius of ~1 mm and the orthogonal minor axis radius of <0.3 mm. It moves northwest during southern Summer and southeast six months later; (2) the continent is tilted northwest in Summer and southeast in Winter, creating the vertical slope across the continent by <5 mm over ~3,500 km.

In Australia, the CM deformation is even larger than the local hydrological, oceanic, atmospheric load deformation in horizontal displacement, while it is 2–3 times smaller in vertical displacement. The Australian continent happens to be located between the peaks and troughs of the global mean (degree-1) surface mass or, in other words, where the horizontal gradient of the degree-1 surface mass is largest. Therefore, it is subject to the largest horizontal motion caused by the degree-1 loading among other countries.

A simple method was demonstrated to estimate the CM motion based on a combination of GPS and GRACE data by exploiting the fact that GRACE is insensitive to the

CM motion but sensitive to other local (high degree components) loading while GPS is sensitive to all components of loading. The same idea has been exploited by *Davis et al*. [2004] and *Swenson et al.* [2008]. This study showed that even the regional set of GPS data (3D positions) can provide full constraints on the CM motion. The systematic errors caused by different data processing strategies associated with spherical harmonic truncation and the J2 uncertainty in the GRACE data were found relatively insignificant, compared to the size of CM signals, as long as the GRACE data up to degree and order 40 are taken. The GRACE data are accurate enough to remove local (other than degree 1) loading effects from GPS in Australia.

The systematic errors related to GPS tropospheric delay modeling are of less concern for the CM determination. However, I found that the GPS/GRACE CM estimates present most likely non-geophysical signal at the frequency of twice per the GPS draconitic year. No signal at such frequency is observed from SLR geocenter solutions. Both GPS/GRACE and SLR solutions reveal the CM solutions largest at the annual cycle (365.25 days) that is distinguished from the GPS draconitic period (351.4 days). The CM motion is the most dominant signal in GPS – GRACE observations of the degree-1 displacement. Stacking multiple GPS data sets corrected with GRACE data into the CM coordinates effectively reduces data noise mostly in the GPS data. The method can be extended to process GPS data from other regions as well as globally, which will improve the resolution of the CM motion against GPS systematic errors.

In this study, GPS displacement and GRACE gravity change are attributed to the result of surface mass loading on the elastic Earth. The tectonic and earthquakes signals existing in GPS data make it difficult to determine particularly the inter-annual change in the CM variations. The seasonal displacements induced by surface temperature change are computed to be 1–2 mm at a regional spatial scale [*Fang et al*., 2014] and will bias the CM

motion determination. The Earth‟s variable structures and rheological properties, departing from a simple laterally homogeneous elastic Earth‟s model used in this study, will influence surface deformations as well as geopotential fields [*e.g.*, *Dill et al*., 2015]. More complex and comprehensive mechanical models of the realistic Earth‟s response should be developed to understand geodetic data for global and regional load deformation [*e.g.*, *Sauber et al., 2014*].

GPS deformation measurements are being increasingly exploited to study terrestrial water and ice mass storage through load deformation calculation [*e.g.*, *Fu et al.*, 2013; *Argus et al*., 2014; *Borsa et al*., 2014]. When the surface loading is known such as tides, the GPS measurements can also be used to infer the Earth‟s structure [*e.g.*, *Marten et al*., 2016]. These geodetic approaches should be meaningful only with proper understanding of the CM-induced deformation in GPS data that may amount to be even larger than the local hydrology and ocean loading. *Ries* [2013] and *Melachroinos et al*. [2013] emphasized the importance of having models of annual geocenter motions for accurate sea level determination to improve satellite orbits. This study demonstrates a kinematic way of determining seasonal CM motions independently from the dynamic method based on gravity and orbit analysis of SLR satellites.

Acknowledgement

This work was funded by University of Newcastle to support NASA"s GRACE and GRACE Follow-On missions. I thank DLR for GRACE telemetry data and JPL, CSR, and GFZ for high-quality Level-1B and Level-2 data. I thank Jürgen Kusche and Xiaoping Wu for clarification on the reference frame and the degree-1 coefficients. I thank Karl Bretreger for proofreading the manuscript. The constructive comments by Paul Tregoning (Editor), Associate Editor, Matt King and an anonymous reviewer were helpful to improve the original manuscript substantially. GRACE data used in this study are available from http://podaac.jpl.nasa.gov/GRACE and http://grgs.obs-mip.fr/grace. Two different GPS position solutions are obtained from http://geodesy.unr.edu and https://gipsy-oasis.jpl.nasa.gov. SLR geocenter data are used from ftp.csr.utexas.edu/pub/slr/geocenter.

Reference

Argus, D. F., Y. Fu, and F. W. Landerer (2014), Seasonal variation in total water storage in California inferred from GPS observations of vertical land motion, Geophys. Res. Lett., 41, 1971–1980, doi:10.1002/2014GL059570.

Bettadpur et al. (2014), CSR Level-2 Status, a paper presented at GRACE Science Team Meeting, Potsdam, Germany, September 29-31, 2014

Blewitt, G., D. Lavallee, P. Clarke, and K. Nurutdinov (2001), A new global mode of Earth deformation: Seasonal cycle detected, Science, 294, 2342–2345.

Blewitt, G. (2003), Self-consistency in reference frames, geocenter definition, and surface loading of the solid Earth, J. Geophys. Res., 108(B2), 2103, doi:10.1029/2002JB002082.

Blewitt, G., and P. Clarke, Inversion of Earth"s changing shape to weigh sea level in static equilibrium with surface mass redistribution, J. Geophys. Res., 108(B6), 2311, doi:10.1029/2002JB002290, 2003.

Blewitt, G., C. Kreemer, W.C. Hammond, J. Gazeaux, 2016, MIDAS robust trend estimator for accurate GPS station velocities without step detection, accepted for publication in the Journal of Geophysical Research, doi: 10.1002/2015JB012552.

Boehm, J., B. Werl, and H. Schuh (2006), Troposphere mapping functions for GPS and very long baseline interferometry from European Centre for Medium-Range Weather Forecasts operational analysis data, J. Geophys. Res., 111, B02406, doi:10.1029/2005JB003629.

Borsa, A. A., D. C. Agnew, and D. R. Cayan (2014), Ongoing drought-induced uplift in the western United States, *Science*, 345.

Chao, B. F., W. P. O'Connor, A. T. C. Chang, D. K. Hall, and J. L. Foster, Snow-load effect on the Earth's rotation and gravitational field, 1979-1985, *J. Geophys. Res., 92,* 9415-9422, 1987.

Chen, J.L., C.R. Wilson, R.J. Eanes, and R.S. Nerem, Geophysical Interpretation of Observed Geocenter Variations, J. Geophy. Res., Vol. 104, No. B2, 2683 - 2690, 1999.

Cheng, M., Ries, J., Tapley, B., 2010. Geocenter variations from analysis of SLR data. In: IAG Commission 1 Symposium 2010, Reference Frames for Applications in Geosciences (REFAG2010), Marne-La-Vallée, France, 4-8 October.

Cheng, M.K., J.C. Ries, B.D. Tapley (2013) Geocenter Variations from Analysis of SLR data, in Reference Frames for Applications in Geosciences, International Association of Geodesy Symposia, Vol. 138, 19-26 (Springer-Verlag Berlin Heidelberg).

Davis, . L., P. Elo seguį J. X. Mitrovica, and M. E. Tamisiea (2004), Climate-driven deformation of the solid Earth from GRACE and GPS, Geophys. Res. Lett., 31, L24605, doi:10.1029/2004GL021435.

Dill, R., V. Klemann, Z. Martinec and M. Tesauro 2015. Applying local Green's functions to study the influence of the crustal structure on hydrological loading displacements. Journal of Geodynamics, 88(0): 14-22, doi:10.1016/j.jog.2015.04.005.

Dobslaw, H., Flechtner, F., Bergmann-Wolf, I., Dahle, Ch., Dill, R., Esselborn, S., Sasgen, I., Thomas, M. (2013), Simulating High-Frequency Atmosphere-Ocean Mass Variability for De- Aliasing of Satellite Gravity Observations: AOD1B RL05, J. Geophys. Res., 118(C5), 10.1002/jgrc.20271.

Fang, M., D. Dong and B.H. Hager 2014. Displacements due to surface temperature variation on a uniform elastic sphere with its centre of mass stationary. Geophysical Journal International, 196(1): 194-203, doi:10.1093/gji/ggt335.

Farrell, W. E. (1972), Deformation of the Earth by surface loads, Rev. Geophys., 10, 761–797.

Fu, Y., D. F. Argus, J. T. Freymueller, and M. B. Heflin (2013), Horizontal motion in elastic response to seasonal loading of rain water in the Amazon Basin and monsoon water in Southeast Asia observed by GPS and inferred from GRACE, Geophys. Res. Lett., 40, 6048–6053, doi:10.1002/2013GL058093.

Han, S.-C., D. D. Rowlands, S. B. Luthcke, and F. G. Lemoine (2008), Localized analysis of satellite tracking data for studying time-variable Earth‟s gravity fields, . Geophys. Res., 113, B06401, doi:10.1029/2007JB005218.

Han, S.-C., R. Riva, J. Sauber, and E. Okal (2013), Source parameter inversion for recent great earthquakes from a decade-long observation of global gravity fields, J. Geophys. Res. Solid Earth, 118, 1240–1267, doi:10.1002/jgrb.50116.

Heiskanen W. A. and Moritz H. (1967), Physical Geodesy, W. H. Freeman and Co., San Francisco-London.

Jekeli, C. (2015): Potential Theory and the Static Gravity Field of the Earth. *Treatise on Geophysics*, Elsevier.

Kusche, J., and E. J. O. Schrama (2005), Surface mass redistribution inversion from global GPS deformation and Gravity Recovery and Climate Experiment (GRACE) gravity data, J. Geophys. Res., 110, B09409, doi:10.1029/2004JB003556.

Lemoine, J.-M., S. Bruinsma, P. G gout, R. Biancale, S. Bourgogne (2014), Release 3 of the GRACE gravity solutions from CNES/GRGS, a paper presented at GRACE Science Team Meeting, Potsdam, Germany, September 29-31, 2014.

Martens, H., M. Simons, S. Owen, and L. Rivera (2016), Observations of ocean tidal load response in South America from subdaily GPS positions, Geophys. J. Int. (2016) 205, 1637–1664.

Melachroinos et al. (2013), The effect of geocenter motion on Jason-2 orbits and the mean sea level, Advances in Space Research, 51(8), 1323–1334, DOI: 10.1016/j.asr.2012.06.004

Nahmani, S., et al. (2012), Hydrological deformation induced by the West African Monsoon: Comparison of GPS, GRACE and loading models, J. Geophys. Res., 117, B05409, doi:10.1029/2011JB009102.

Pavlis, E. (2003), The SLR Contribution to the ITRF Monitoring the Origin of the TRF with Space Geodetic Techniques, in Proceedings From the Science Session and Full Proceedings CD-ROM, edited by Ron Noomen, Steven Klosko, Carey Noll, and Michael Pearlman, NASA/CP-2003-212248, 2003.

Ray, J., Z. Altamimi, X. Collieux, and T. van Dam (2008), Anomalous harmonics in the spectra of GPS position estimates, GPS Solut., 12, 55–64, doi:10.1007/s10291-007-0067-7.

Ries, J. (2013), Seasonal Geocenter Motion from Space Geodesy and Models, a paper presented at IERS Retreat 23-24 May 2013 Paris, France

Rodell, M., P. R. Houser, U. Jambor, J. Gottschalck, K. Mitchell, C.-J. Meng, K. Arsenault, B. Cosgrove, J. Radakovich, M. Bosilovich, J. K. Entin, J. P. Walker, D. Lohmann, and D. Toll, The Global Land Data Assimilation System, Bull. Amer. Meteor. Soc., 85(3): 381-394, 2004.

Sauber, J., S.-C. Han, S. Luthcke, N. Ruppert, R. Bruhn (2014), Measurement and Modeling of Cryosphere-Geosphere Interactions in South Central Alaska, American Geophysical Union, Fall Meeting 2014, abstract #G51A-0338.

Steigenberger, P., J. Boehm, and V. Tesmer (2009), Comparison of GMF/ GPT with VMF1/ECMWF and implications for atmospheric loading, J. Geod., doi:10.1007/s00190-009-0311-8.

Swenson, S., D. Chambers, and J. Wahr 2008 Estimating geocenter variations from a combination of GRACE and ocean model output, J. Geophys. Res., 113, B08410, doi:10.1029/2007JB005338.

Tregoning, P. (2003), Is the Australian Plate deforming? A space geodetic perspective, Geological Society of America Special Papers, 2003, 372, p. 41-48.

Tregoning, P., R. Burgette, S. C. McClusky, S. Lejeune, C. S. Watson, and H. McQueen (2013), A decade of horizontal deformation from great earthquakes, J. Geophys. Res. Solid Earth, 118, 2371–2381, doi:10.1002/jgrb.50154.

Tregoning, P. and C. Watson (2009), Atmospheric effects and spurious signals in GPS analyses, J. Geophys. Res., 114, B09403, doi:10.1029/2009JB006344.

Wahr, J., S. A. Khan, T. van Dam, L. Liu, J. H. van Angelen, M. R. van den Broeke, and C. M. Meertens (2013), The use of GPS horizontals for loading studies, with applications to northern California and southeast Greenland, J. Geophys. Res. Solid Earth, 118, 1795–1806, doi:10.1002/jgrb.50104.

Watkins, M., et al. (2015), Improved methods for observing Earth's time variable mass distribution with GRACE using spherical cap mascons. *J. Geophys. Res*, 120, 2648-2671.

Wu, X., D. F. Argus, M. B. Heflin, E. R. Ivins, and F. H. Webb (2002), Site distribution and aliasing effects in the inversion for load coefficients and geocenter motion from GPS data, Geophys. Res. Lett., 29(24), 2210, doi:10.1029/2002GL016324.

Wu, X., M. B. Heflin, E. R. Ivins, and I. Fukumori (2006), Seasonal and interannual global surface mass variations from multisatellite geodetic data, J. Geophys. Res., 111, B09401, doi:10.1029/2005JB004100.

Wu, X., J. Ray, T. van Dam (2012), Geocenter motion and its geodetic and geophysical implications, Journal of Geodynamics 58 (2012) 44–61

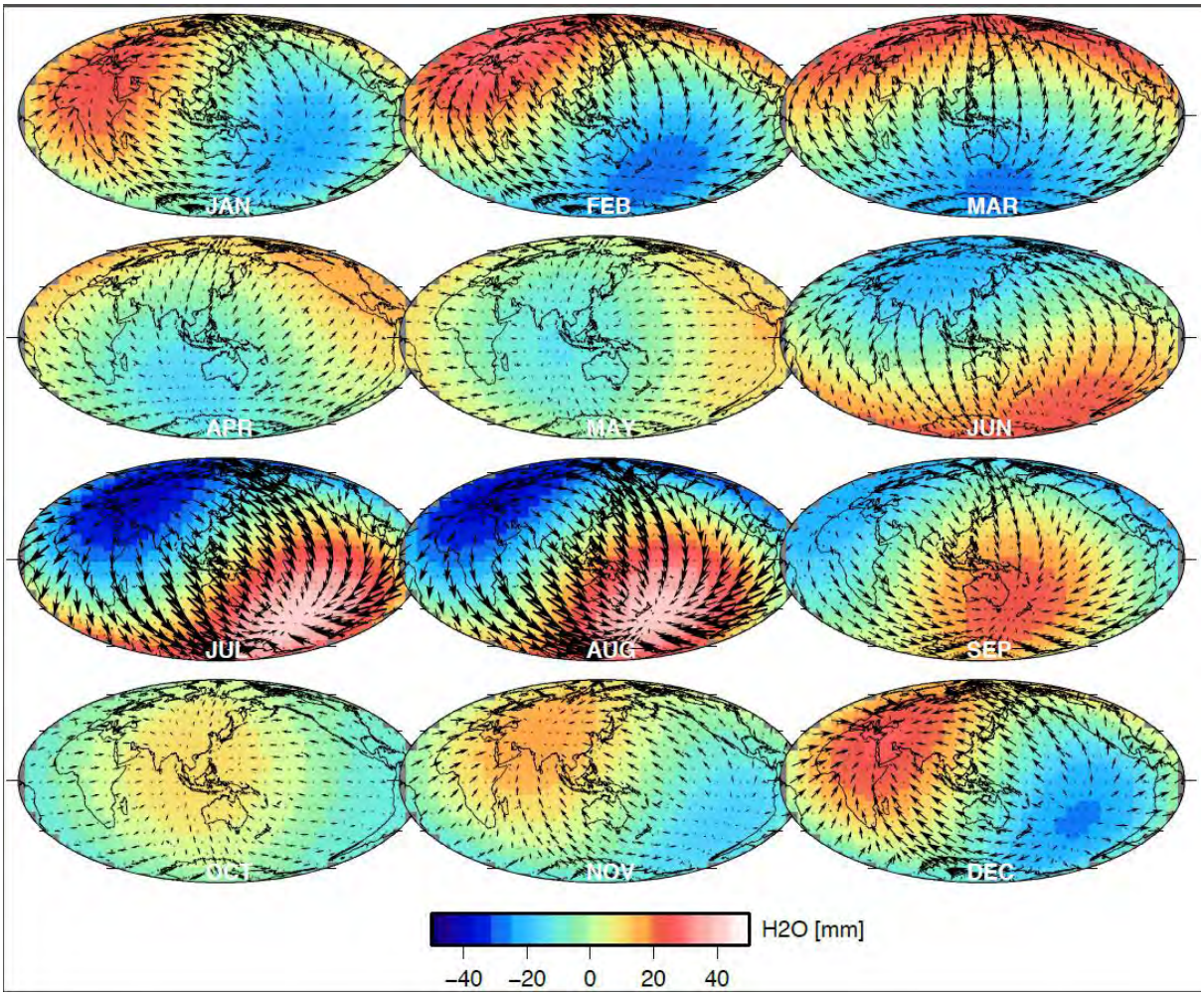

Figure 1. Monthly maps of globally-averaged (*i.e.*, „degree-1“) surface mass redistribution quantified in terms of equivalent water height. The SLR-determined geocenter motions were interpreted as a result of mass redistribution on the surface and the accompanying load deformation. Monthly snapshots were calculated by stacking multi-years of SLR geocenter estimates after removing linear trends in the estimates. The arrows indicate the horizontal displacements induced by the Earth“s elastic response to the surface mass load (the longest arrow corresponds to the largest movement of ~1 mm). The vertical displacement is identical to these maps but with a scale factor of -0.05 (See the text).

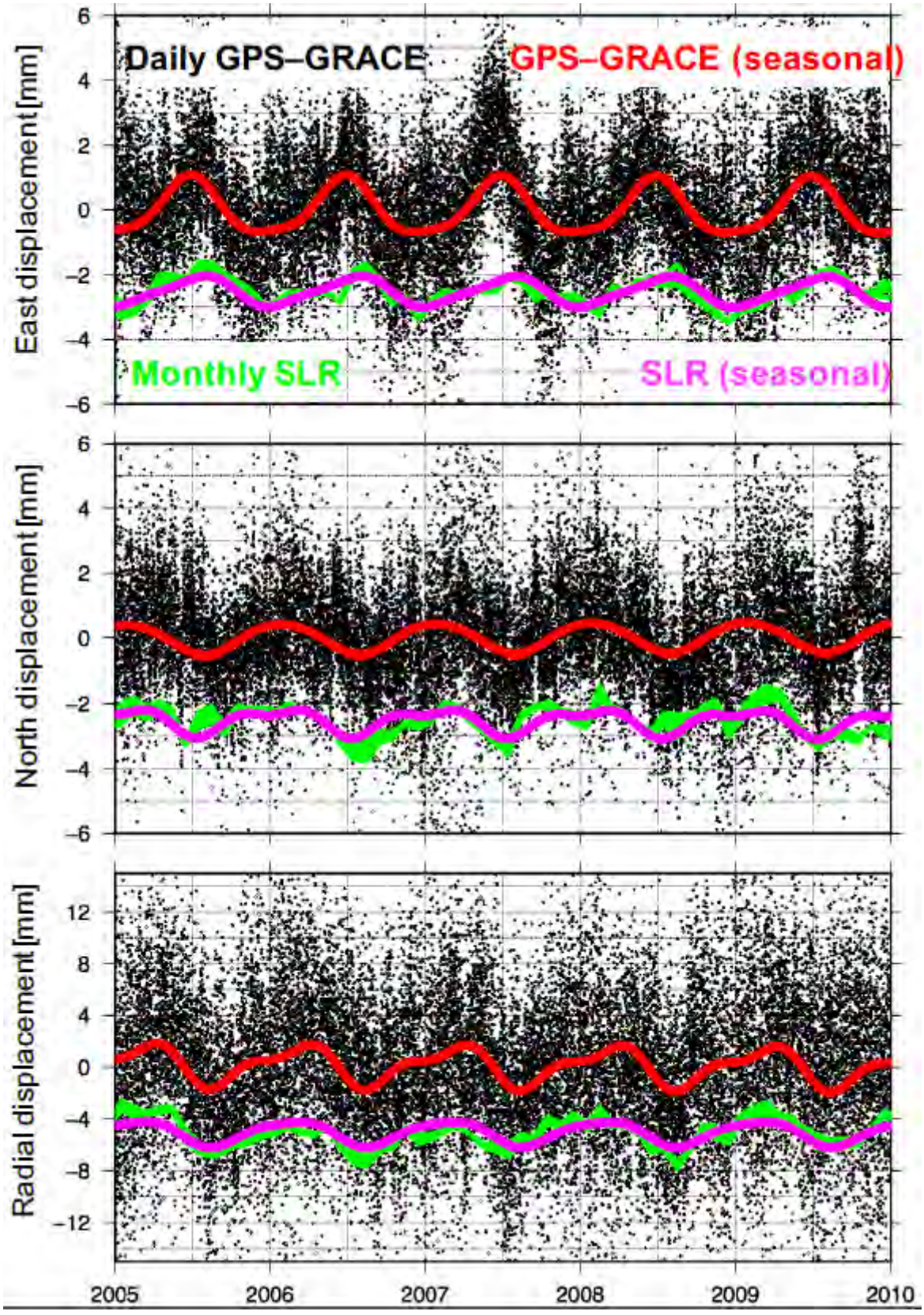
Daily GPS–GRACE
GPS–GRACE (seasonal)
Monthly SLR
SLR (seasonal)
East displacement [mm]
North displacement [mm]
Radial displacement [mm]
6
4
2
0
−2
−4
−6
12
8
−8
−12
2005
2006
2007
2008
2009
2010

Figure 2. Daily load displacements caused by the degree-1 ($l = 1$) surface mass were determined using the GPS displacements from 14 stations in Australia after removing the GRACE-inferred local ($l \geq 2$) load displacements (black dots). The de-trended monthly degree-1 load displacements evaluated at GPS stations using the SLR geocenter motions are shown in green solid lines. The seasonal components (annual and semi-annual sinusoids) were determined from each time-series of GPS-GRACE and SLR, respectively, shown in red and magenta solid lines. The geographic locations of 14 GPS stations are shown in Figure 3.

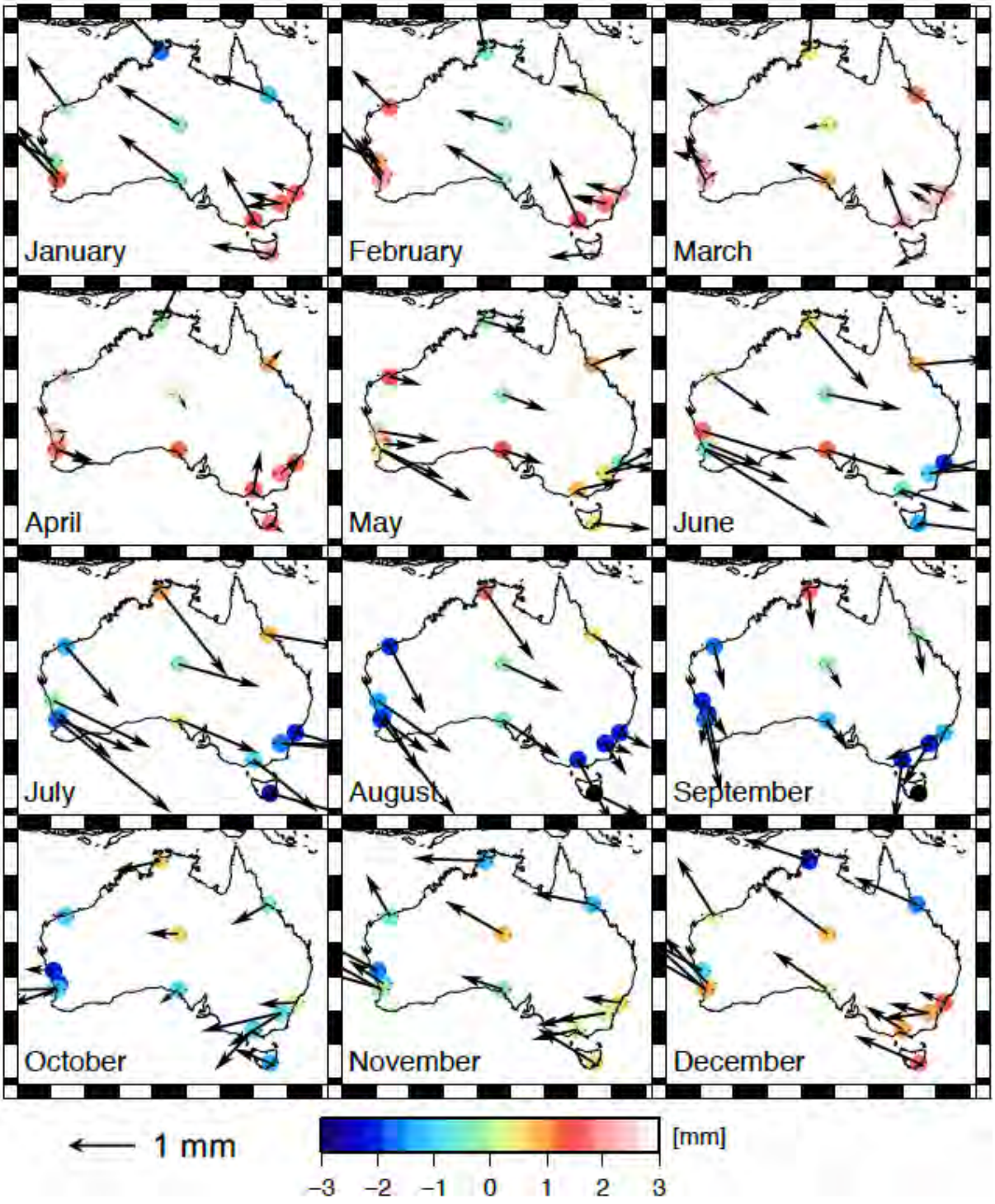

Figure 3. Monthly patterns of 3D displacements induced by the degree-1 surface mass loading were determined by the difference between GPS and GRACE data. The time-series of GPS and GRACE displacement data from 2003 to 2015 were de-trended and stacked to

estimate the monthly patterns of deformation at each station. The vertical and horizontal displacements are shown with colored dots and the solid black arrows, respectively.

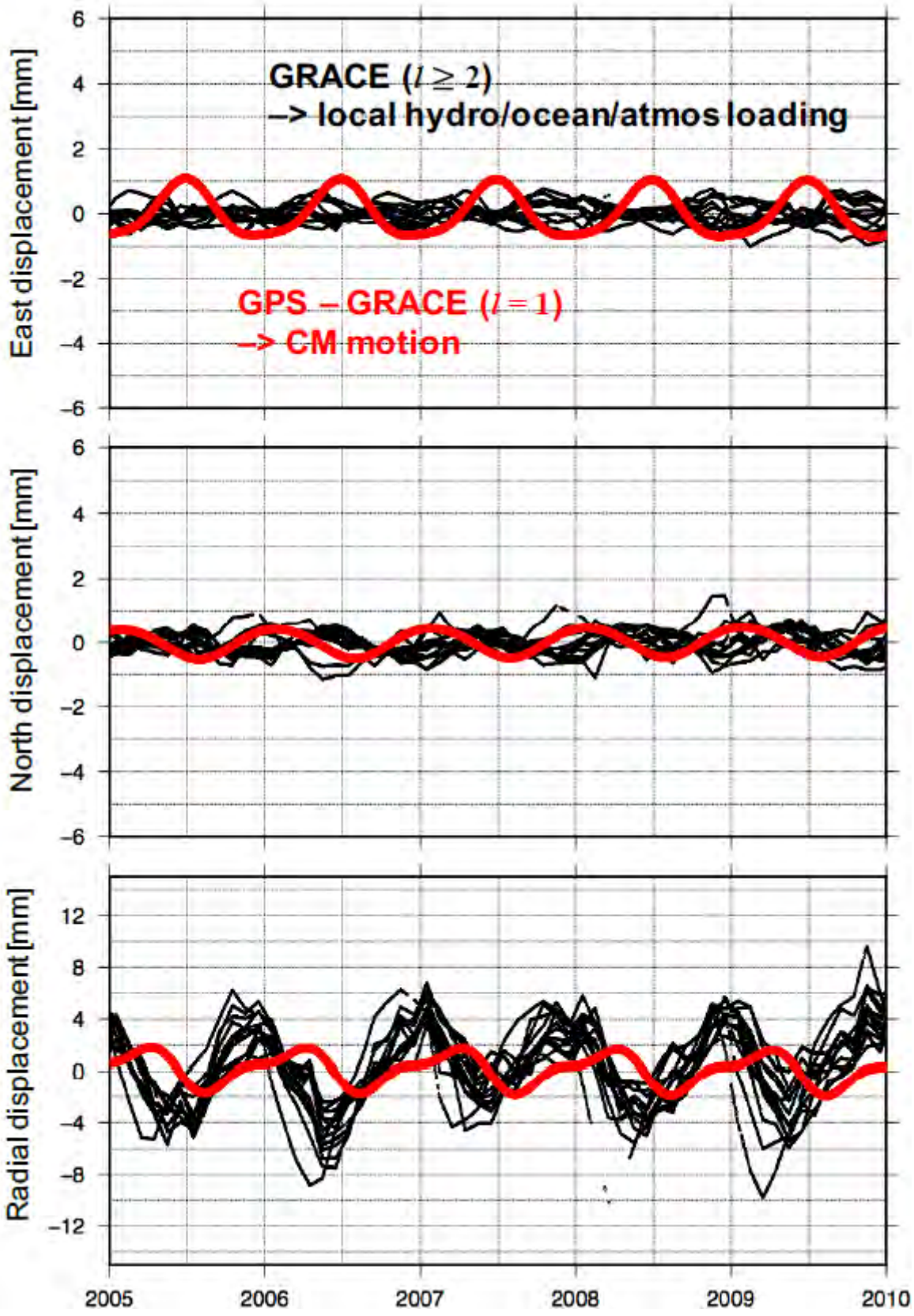
GRACE ($l \geq 2$)
–> local hydro/ocean/atmos loading
GPS – GRACE ($l = 1$)
–> CM motion
East displacement [mm]
North displacement [mm]
Radial displacement [mm]
6
4
2
0
–2
–4
–6
12
8
–8
–12
2005
2006
2007
2008
2009
2010

Figure 4. The time-series of load displacements due to local ($l \geq 2$) hydrologic, atmospheric, and oceanic loads, evaluated at 14 GPS stations using GRACE (black). The spherical harmonic degree and order up to 40 were used for GRACE data. They are compared with the estimated seasonal motion of the degree-1 displacements from GPS minus GRACE, averaged from all 14 stations in Australia (red, the same as Figure 2).

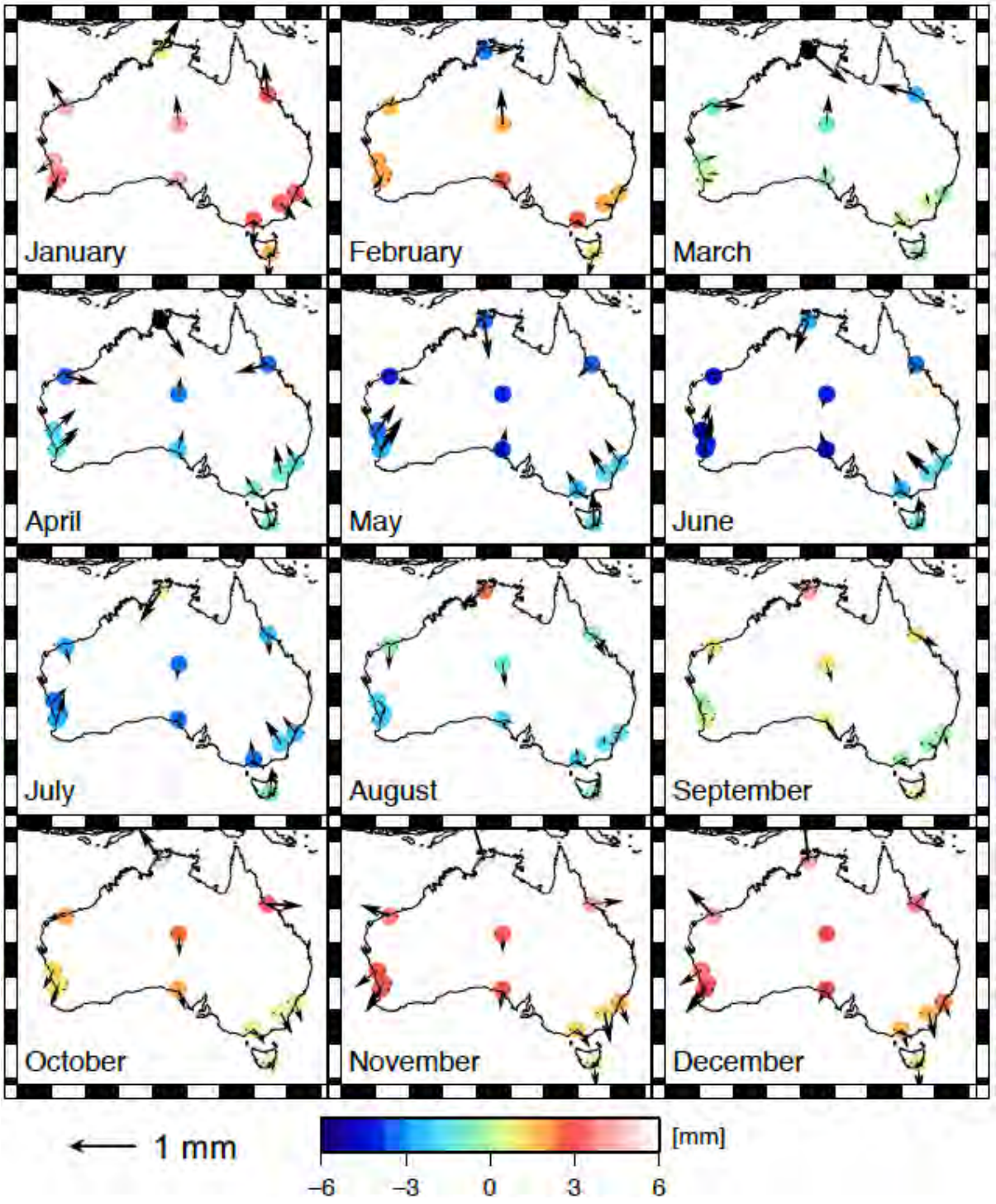

Figure 5. Monthly patterns of 3D displacements induced by the local hydrologic, and atmospheric, and oceanic loads estimated from GRACE data. The time-series of GRACE displacement data from 2003 to 2015 were de-trended and stacked to estimate the monthly

patterns of deformation at each station. The vertical and horizontal displacements are shown with colored dots and the solid black arrows, respectively.

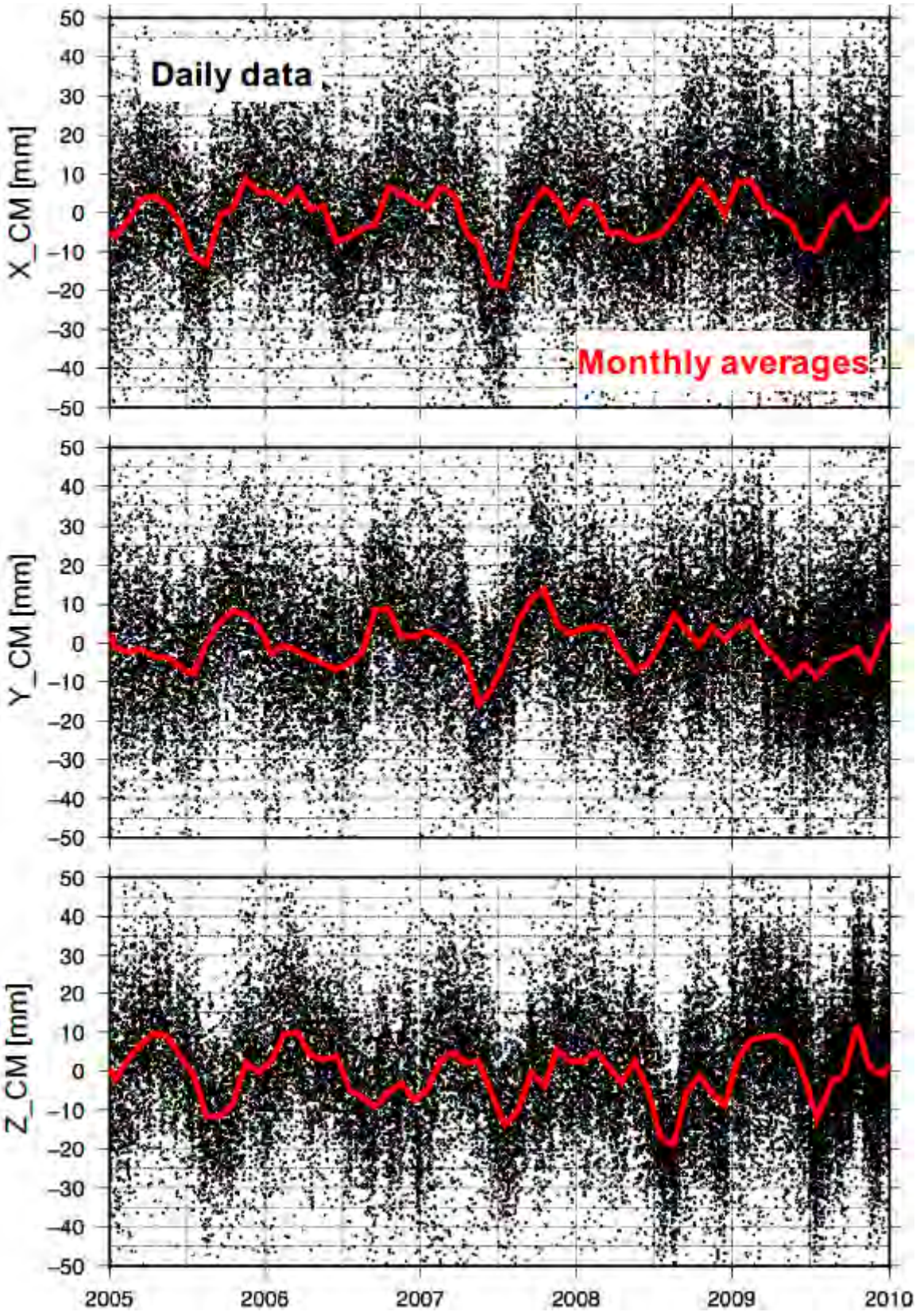
Daily data
Monthly averages
X_CM [mm]
Y_CM [mm]
Z_CM [mm]
50
40
30
20
10
0
−10
−20
−30
−40
−50
2005
2006
2007
2008
2009
2010

Figure 6. Daily time-series of the CM coordinates, X_{CM}, Y_{CM}, and Z_{CM} (*i.e.*, geocenter motion) were estimated by inverting the differences of GPS and GRACE data (black dots). The monthly averages of the daily estimates were also calculated (red dots).

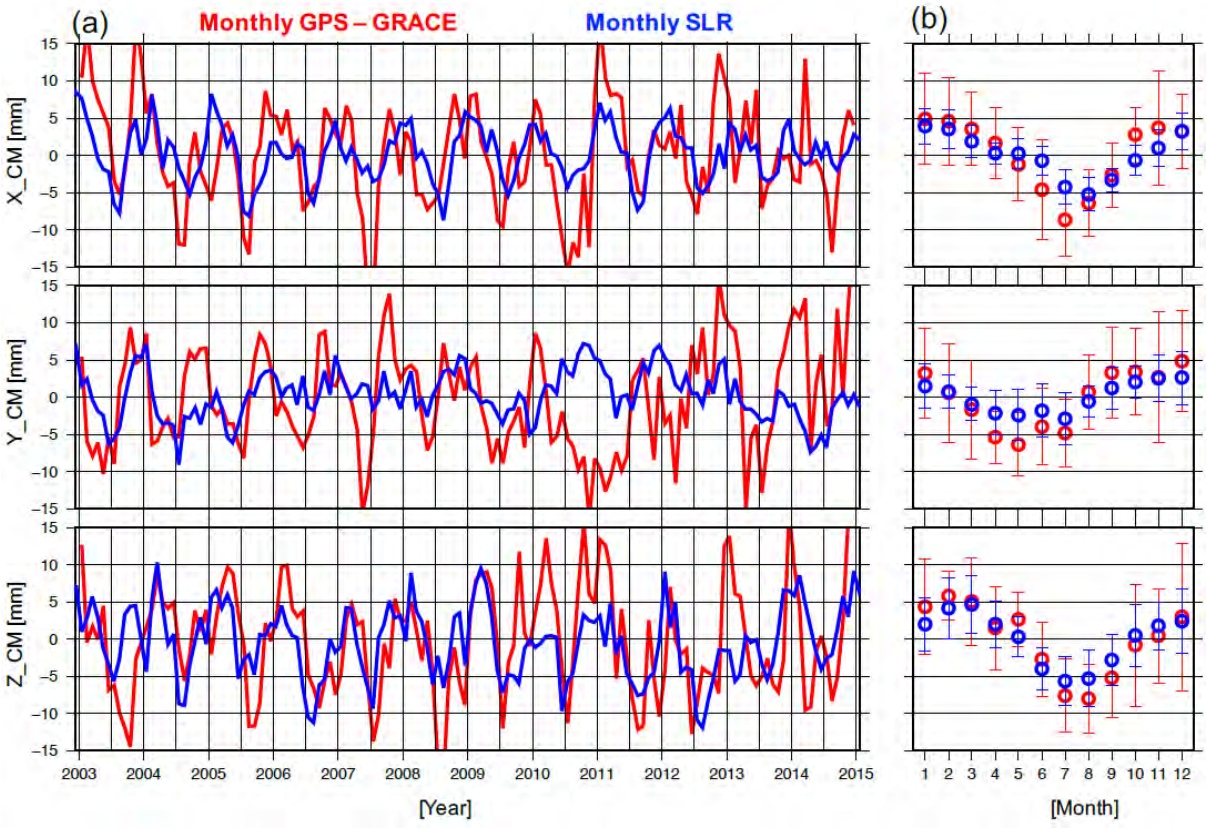

Figure 7. (a) Comparison of the monthly estimates of the CM coordinates in 2003–2015 from GPS–GRACE (red) and SLR geocenter solutions (blue). (b) The average monthly variations of the CM coordinates during 2003–2015 from GPS–GRACE and SLR. The error bar indicates the standard deviation of the variations from the average in each month over 2003–2015.

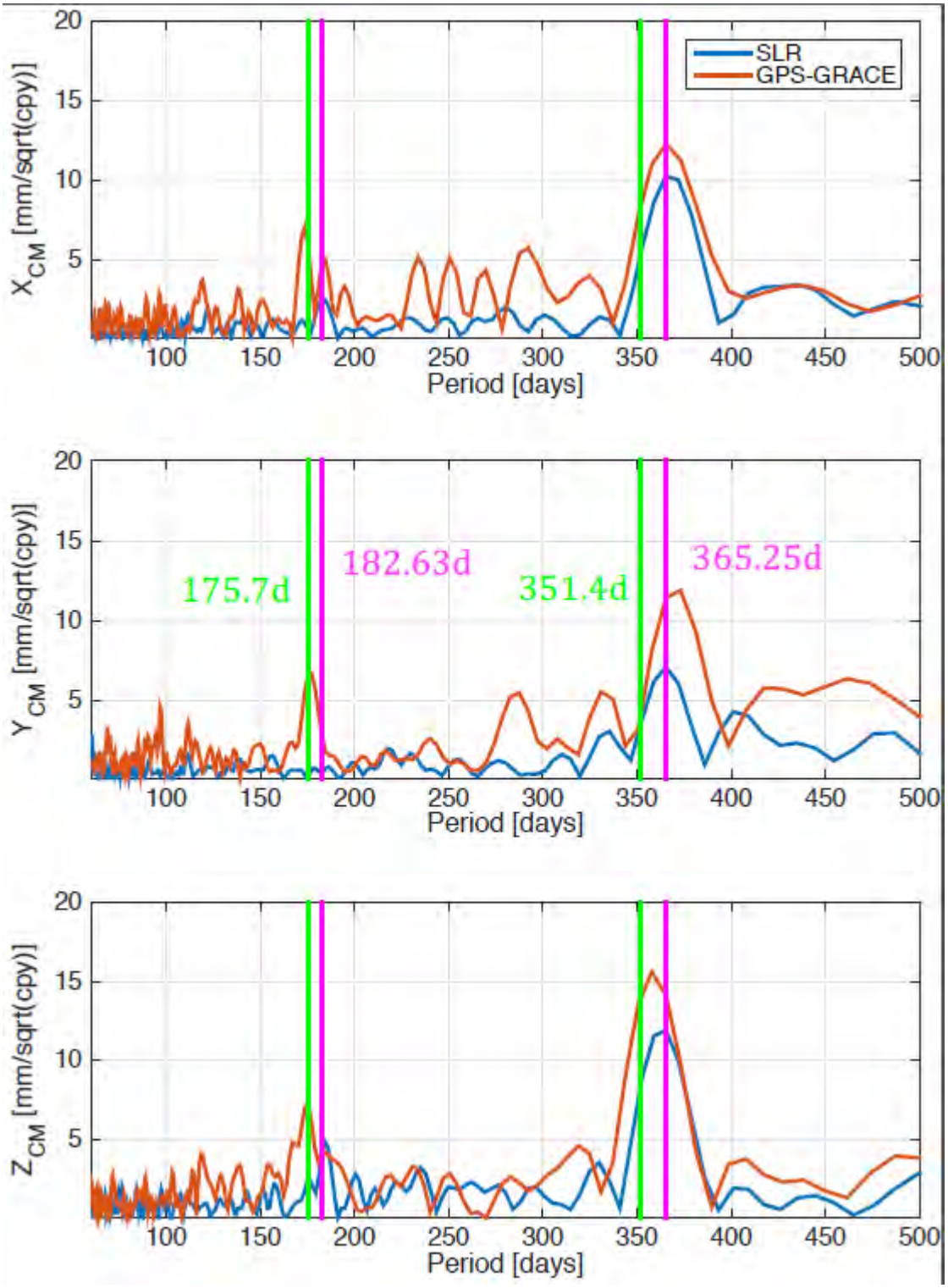

Figure 8. The amplitude (square root of power) spectral density of monthly time-series of the CM motion estimates from this study and the SLR analysis. The magenta vertical bars

indicate the periods of the solar year (365.25 days) and its half (182.63 days). The green vertical bars indicate those of GPS draconitic year (351.5 days) and its half (175.7 days).

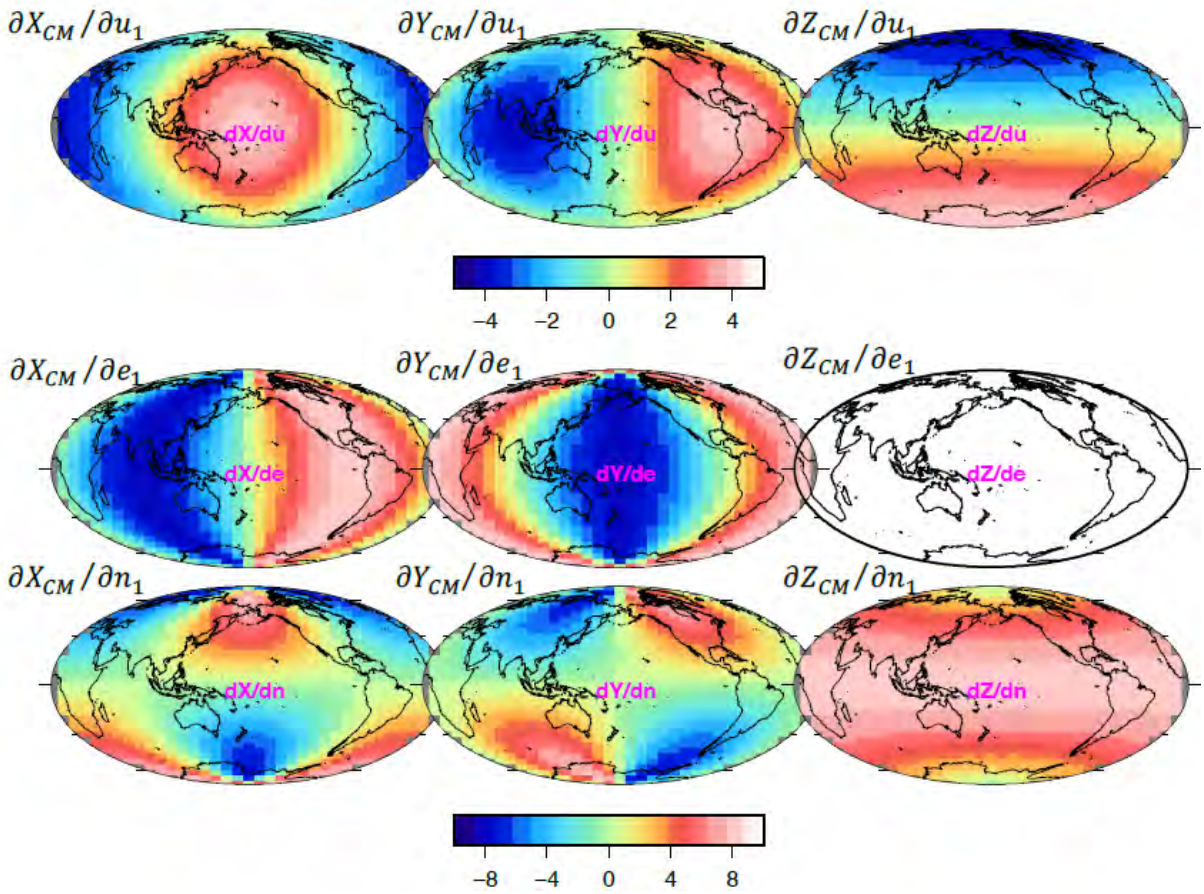

Figure 9. The sensitivities (partial derivatives) of the CM coordinates with respect to the degree-1 displacements. All nine components were computed from the matrix $^{-1}(\theta, \lambda)$ of equation (10). Note two different scale bars for the sensitivity to the vertical motion and to the horizontal motion.

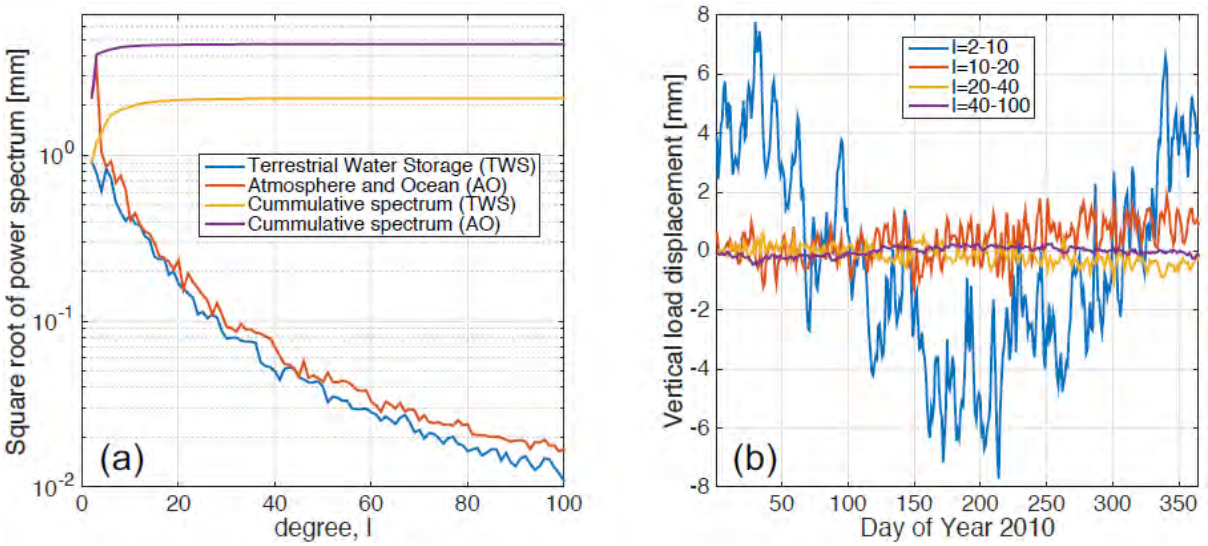

Figure 10. (a) The degree amplitude spectrum and the cumulative spectrum of the vertical load displacement computed from hydrology, atmosphere and ocean models. (b) Daily time-series of the synthetic displacements of atmosphere and ocean mass loads, computed at different degree bands, evaluated at the central Australia (Alice Spring).

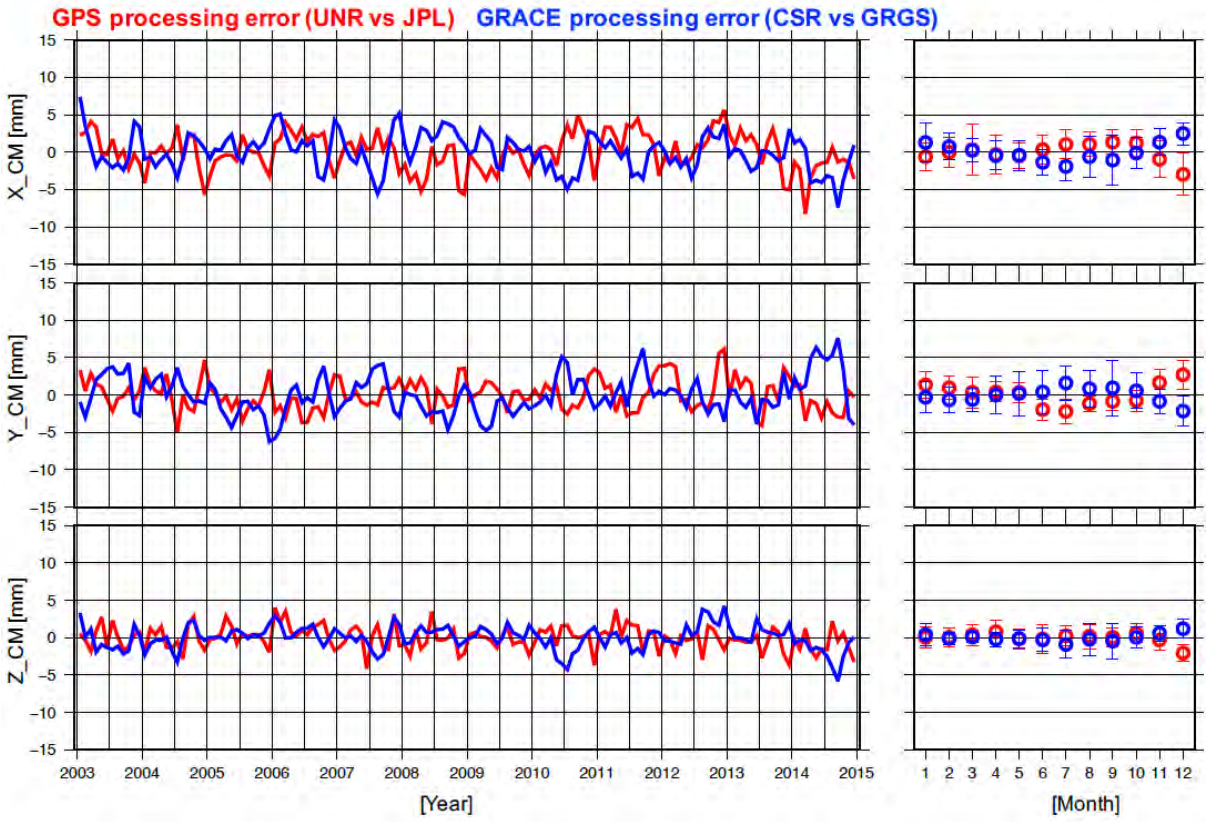

Figure 11. Similar to Figure 7, but they represent the effects of GPS and GRACE data processing errors (difference between two GPS solutions and between two GRACE solutions) on the CM coordinates.